Probing plasma membrane microdomains in cowpea protoplasts using lipidated GFP-fusion proteins and multimode FRET microscopy

Vermeer, J.E.M.; van Munster, E.B.; Vischer, N.O.; Gadella, T.W.J.

DOI
10.1111/j.0022-2720.2004.01318.x

Publication date
2004

Document Version
Final published version

Published in
Journal of Microscopy

Journal of Microscopy, Vol. 214, Pt 2 May 2004, pp. 190–200
Received 26 June 2003; accepted 8 December 2003

Probing plasma membrane microdomains in cowpea protoplasts using lipidated GFP-fusion proteins and multimode FRET microscopy

J. E. M. VERMEER, E. B. VAN MUNSTER, N. O. VISCHER & T. W. J. GADELLA JR
Section Molecular Cytology, Centre for Advanced Microscopy, Swammerdam Institute for Life Sciences, University of Amsterdam, Kruislaan 316, 1098 SM, Amsterdam, the Netherlands

Key words. Acceptor bleaching, FLIM, FRET–FRAP, FRET microscopy, GFP, lipid microdomains, spectral imaging.

Summary

Multimode fluorescence resonance energy transfer (FRET) microscopy was applied to study the plasma membrane organization using different lipidated green fluorescent protein (GFP)-fusion proteins co-expressed in cowpea protoplasts. Cyan fluorescent protein (CFP) was fused to the hyper variable region of a small maize GTPase (ROP7) and yellow fluorescent protein (YFP) was fused to the N-myristoylation motif of the calcium-dependent protein kinase 1 (*Le*CPK1) of tomato. Upon co-expressing in cowpea protoplasts a perfect co-localization at the plasma membrane of the constructs was observed. Acceptor-photobleaching FRET microscopy indicated a FRET efficiency of 58% in protoplasts co-expressing CFP-Zm7hvr and myrLeCPK1-YFP, whereas no FRET was apparent in protoplasts co-expressing CFP-Zm7hvr and YFP. Fluorescence spectral imaging microscopy (FSPIM) revealed, upon excitation at 435 nm, strong YFP emission in the fluorescence spectra of the protoplasts expressing CFP-Zm7hvr and myrLeCPK1-YFP. Also, fluorescence lifetime imaging microscopy (FLIM) analysis indicated FRET because the CFP fluorescence lifetime of CFP-Zm7hvr was reduced in the presence of myrLeCPK1-YFP. A FRET fluorescence recovery after photobleaching (FRAP) analysis on a partially acceptor-bleached protoplast co-expressing CFP-Zm7hvr and myrLeCPK1-YFP revealed slow requenching of the CFP fluorescence in the acceptor-bleached area upon diffusion of unbleached acceptors into this area. The slow exchange of myrLeCPK1-YFP in the complex with CFP-Zm7hvr reflects a relatively high stability of the complex. Together, the FRET data suggest the existence of plasma membrane lipid microdomains in cowpea protoplasts.

Correspondence to: Professor Theodorus W. J. Gadella Jr. Tel.: +31 20 525 6259; fax: +31 20 525 6271; e-mail: gadella@science.uva.nl

Introduction

The introduction of green fluorescent protein (GFP) as a genetic encoded fluorescent marker has greatly accelerated the study of protein localization. GFP has enabled non-invasive, real-time microscopic imaging of living cells. With the introduction of cyan-emitting (CFP) and yellow-emitting (YFP) GFP variants, GFP-based fluorescence resonance energy transfer (FRET) microscopy has become possible (Tsien, 1998). CFP and YFP form an excellent FRET pair and thus have enabled the study of protein–protein interactions (Sorkin *et al.*, 2000; Janetopoulos *et al.*, 2001) and the study of second messengers using conformational change-based indicators (Honda *et al.*, 2001; Miyawaki *et al.*, 1997) in living cells. Also in plant research, GFP-based FRET microscopy has been applied for such studies (Gadella *et al.*, 1999; Immink *et al.*, 2002).

FRET is a quantum mechanical phenomenon that can be defined as the radiationless transmission of an energy quantum from a fluorescent molecule to a chromophore in its close proximity through dipole–dipole coupling. The distance over which this phenomenon will occur is usually < 100 Å (Gadella *et al.*, 1999). FRET is characterized by a quenched donor fluorescence, which occurs in parallel with an increase of acceptor fluorescence (if the acceptor is a fluorophore). The increased acceptor fluorescence is called sensitized emission. The FRET efficiency (E) is defined in Eq. (1), in which I_D is the intensity of the donor (i.e. CFP) in the absence of the acceptor (i.e. YFP) and I_{DA} is the intensity of the donor in the presence of the acceptor. The relationship between FRET efficiency (E) and the actual distance (r) between a single donor and a single acceptor molecule is given in the Förster Eq. (2), showing that FRET can also be used to estimate the approximate distances between the donor and the acceptor chromophores (Stryer, 1978).

$$E \equiv 1 - \frac{I_{DA}}{I_D} = 1 - \frac{\bar{\tau}_{DA}}{\bar{\tau}_D} \qquad (1)$$

$$E = \frac{1}{1 + \left(\frac{r}{R_0}\right)^6}. \quad (2)$$

In Eq. (1) $\bar{\tau}_{DA}$ and $\bar{\tau}_D$ are the average fluorescence lifetimes of the donor in the presence and absence of the acceptor, respectively. In Eq. (2) R_0 is the Förster radius for FRET, which depends on the spectral properties and relative orientation of the donor and acceptor molecules (for reviews on FRET see Clegg, 1996; Gadella *et al.*, 1999; Selvin, 2000). For FRET between CFP and YFP R_0 = 5.2 nm (Tsien, 1998; Gadella *et al.*, 1999). FRET can be imaged with the spatial resolution of a microscope using techniques such as fluorescence spectral imaging microscopy (FSPIM) (Gadella *et al.*, 1999; Immink *et al.*, 2002; van Kuppeveld *et al.*, 2002), acceptor bleaching FRET microscopy (Bastiaens *et al.*, 1996; Zaccolo *et al.*, 2000; van der Wal *et al.*, 2001) and fluorescence lifetime imaging microscopy (FLIM) (Gadella & Jovin, 1995; Verveer *et al.*, 2000b; van Kuppeveld *et al.*, 2002). Other methods to measure FRET include various ratio-imaging methods (Sorkin *et al.*, 2000), polarization microscopy methods (Gautier *et al.*, 2001; Clayton *et al.*, 2002) and donor-photo bleaching microscopy (Gadella & Jovin, 1995), but these techniques will not be discussed further here. Some implementations of FRET microscopy are relatively easy whereas other are technically demanding but more robust in terms of (mis)interpretation. The three FRET microscopy methods used in this paper will be discussed below.

Acceptor bleaching FRET microscopy is a relatively easy way to perform FRET microscopy. With this technique, the acceptor is selectively and irreversibly photobleached in an area of the cell by a high-power focused laser beam while leaving the donor intact. This results in an acceptor that no longer can accept the energy from the donor and hence results in dequenching of the donor. By quantifying the increase in donor fluorescence intensity (from I_{DA} to I_D) or the decrease in the lifetime (from $\bar{\tau}_{DA}$ to $\bar{\tau}_D$) the FRET efficiency E can be calculated according to Eq. (1) (Bastiaens *et al.*, 1996). The advantages of acceptor-bleaching are its independence of the chromophore concentration, light path or orientation of structures in the microscope and direct reabsorption of the donor fluorescence by the acceptor or other chromophores (inner filtering). The problems of using acceptor-bleaching are (i) its inherent irreversibility, (ii) the necessity of a selective laser source that is absorbed by the acceptor but not by the donor (e.g. 514 nm Ar-laser for the YFP/CFP couple), (iii) sensitivity of the FRET estimation to CFP-bleaching in taking the donor images before and after bleaching, (iv) movement of the donor molecule between acquisition of the pre- and post-bleach donor images will introduce artefacts and (v) the method is sensitive to photo chromicity of the GFPs that sometimes can be switched to dark (low quantum yield) but absorbing states or to states displaying blue-shifted fluorescence spectra (Creemers *et al.*, 2000). Acceptor-photobleaching is most simply implemented on a confocal microscope incorporating multiple laser excitation lines and at least dual channel detection (Karpova *et al.*, 2003). Acceptor bleaching can also be implemented on wide-field microscopes using arc lamp excitation sources, but in this case special care should be taken so as to select a good bandpass filter for the acceptor bleaching to avoid bleaching of the donor (Kenworthy, 2001). In addition, the speed of bleaching in when using an arc lamp as an excitation source may be so slow that application to living cells is limited.

FSPIM combines spatial resolution with spectral resolution. At every position on a line across the sample a complete spectrum is obtained (Balaban *et al.*, 1986). Using fluorescence spectral imaging microscopy, the sensitized emission can be measured inside living cells and no sequential donor/acceptor images need to be acquired, making the technique relatively insensitive to movement of the specimen. FSPIM is a fast and robust technique for monitoring FRET in living cells. Because it delivers complete emission spectra, it gives a fast qualitative estimate for the presence of FRET. Errors owing to incorrect filter selection, autofluorescence contributions or presence of other dyes are quickly recognized from the shape of the spectra but may be more difficult to see using filter-FRET methods. For comparative FRET studies FSPIM is a particularly fast technique as one can quickly distinguish FRET from non-FRET spectra by monitoring if their shape reveals sensitized emission. However, at high acceptor concentration the direct acceptor excitation at the donor excitation wavelength could yield false-positive FRET signals. In addition, as in any filter-FRET (excitation or emission ratio method), the spectra are sensitive to artefacts related to inner filtering (or reabsorption of emitted photons) yielding reduced observed fluorescence intensities. For plants, absorption by chlorophyll can induce severe inner filtering. For FSPIM measurements, using the CFP/YFP FRET pair, inner filtering by chloroplasts can severely reduce CFP fluorescence (up to 90%), whereas YFP fluorescence is relatively unaffected. In theory, this can give rise to false FRET identification (high YFP/CFP ratio), but with FSPIM, inner filtering reveals itself by causing aberrant CFP spectra that are far more difficult to identify using conventional filter-FRET methods. In addition, because chlorophyll shows strong red autofluorescence upon blue excitation, areas with chlorophyll (and possible inner filtering) are easily detected and in most cases can be avoided in the FSPIM acquisition. The quantitative FRET methods such as FRET–FRAP (discussed above) and FRET–FLIM (discussed below) are not sensitive to inner filtering. Spectral imaging microscopy can be most simply implemented by using an imaging spectrograph coupled to a CCD camera providing spatially resolved emission spectra (Gadella *et al.*, 1997; Goedhart & Gadella, 2000). In addition, several commercial confocal microscopes are on the market enabling spectral detection (Leica-SP, Zeiss-Meta, Biorad-Radiance2100-Rainbow). Care should be taken with confocal systems to acquire the spectra with the least number of excitation scans. Usually the desirable spectral resolution, speed of acquisition and signal-to-noise ration is far better using the spectrograph-CCD systems.

In FLIM–FRET the mean fluorescence lifetime of the donor chromophore is measured, which is typically of the order of nanoseconds (Bastiaens & Squire, 1999; Gadella *et al.*, 1999; Selvin, 2000). In contrast to the above described techniques, FLIM is a kinetic-based technique for determining FRET, in which the excited-state decay kinetics of the donor or fluorescence lifetime (τ_D) is measured. In the presence of an acceptor, the lifetime of the donor (τ_{DA}) will be decreased compared with τ_D (Gadella & Jovin, 1995; Bastiaens & Squire, 1999; Pepperkok *et al.*, 1999; Harpur *et al.*, 2001). The advantage of FLIM over measuring fluorescence intensities is that fluorescence lifetimes are independent of the chromophore concentration, light path and orientation of structures in the microscope, direct reabsorption of the donor fluorescence by the acceptor or other chromophores (inner filtering) and moderate levels of donor photobleaching. Thus, FLIM provides quantitative information on fluorescence energy transfer, thereby avoiding the need for elaborate processing of the obtained data for, for example, concentration differences of the chromophore in the measured samples and light-path length as in filter FRET methods (Gordon *et al.*, 1998). Disadvantages of FRET–FLIM are that setting up the technique is relatively technically demanding and acquisition times (typically 1–10 s) can be problematic in the case of fast movement in living cells (Hanley *et al.*, 2001). Furthermore, with high FRET percentages, donor-lifetime imaging can be relatively insensitive because the signal in this case is generated from strongly quenched donors. In this case sensitized emission lifetime imaging may be of help (Wouters & Bastiaens, 1999). FLIM can be implemented in many different ways using both the time-domain approach or the frequency-domain approach, using both wide-field and confocal microscopes and using both single- and multiphoton excitation. We used the frequency-domain wide-field approach, employing an intensity-modulated laser excitation source and a gain-modulated image intensifier-CCD detection option (van Munster & Gadella, 2004). Other types of FLIM implementations are reviewed elsewhere (Gadella, 1997).

In this study, multimode FRET microscopy was applied to study the existence of plasma membrane lipid–lipid microdomains using lipidated CFP and YFP fusion proteins. We used CFP fused to the C-terminal hyper variable region (HVR) of the maize ROP7 GTPase (Ivanchenko *et al.*, 2000) and YFP modified with the N-myristoylation motif of the calcium-dependent protein kinase 1 (*Le*CPK1) from *Lycopersicum esculentum* (Rutschmann *et al.*, 2002). The HVR targets the proteins to specific membrane compartments (Michaelson *et al.*, 2001), where they function in signal transduction. The best characterized component of the HVR is the CaaX box, a motif of four amino acids at the C-terminus of all described Rho-like GTPases consisting of: C, cysteine; a, aliphatic amino acid; and X, serine, leucine or a methionine. The CaaX box directs membrane-targeting through an isoprenyl group that is attached post-translationally to a cysteine residue near the C-terminus together with one or two palmitoyl anchors attached to internal cysteines when present in the HVR (Glomset & Farnsworth, 1994; Magee & Marshall, 1999). The N-myristoylation motif enables the attachment of a myristoyl anchor to the YFP fusion protein. The chimeras were expressed in cowpea (*Vigna unguiculata*) protoplasts. Using multimode FRET microscopy techniques we show that there is extensive FRET in the plasma membrane between these fusion proteins. These results are consistent with the existence of plasma membrane lipid–lipid microdomains in plant protoplasts.

Materials and methods

Constructs

All constructs were made using standard molecular biological methods (Sambrook & Russel, 2001). To study the expression of proteins and to conduct FRET experiments all constructs were made in the plant expression vector pMON999e35S (Dhonukshe & Gadella, 2003). The plasmid pMG-HVR7, containing GFP fused to the HVR of Maize ROP 7, as described by Ivanchenko *et al.* (2000), was a generous gift from Dr J. E. Fowler (Oregon State University, Corvallis, OR, U.S.A.). For the FRET studies the HVR was cloned behind human codon-optimized CFP (= wtGFP with F64L, S65T, Y66W, N146I, M153T, V163A and N212L) and -YFP (= wtGFP with S65G, V68L, Q69K, S72A and T203Y) (generously provided by G. van der Krogt, Wageningen University, Wageningen, the Netherlands) using PCR with the following primers (restriction sites are in bold type): 5′-GGA**AGATCT**GGGAGGAGGAGGCGAC-3′ and 5′-**GAATTC**CTAAGCAGCGCACGTGCT-3′. The PCR fragments were digested with *Bgl*II and *Eco*RI and cloned in frame behind CFP and YFP in pMON999e35S.

To create the myrLeCPK1-YFP construct, the eight N-terminal amino acids (MGGCFSKK) of *Le*CPK1 (Rutschmann *et al.*, 2002) were fused to YFP by PCR using the following primers (restriction sites are in bold type): 5′-ATG**CCATGG**GAGG-ATGCTTCTCTAAGAAGGTGAGCAAGGGCGAGGAGC-3′ and 5′-GCGGATCCTCACTTGTACAGCTCGTCCATGC-3′. The PCR fragment was digested with *Nco*I and *Bam*HI and cloned in pMON999e35S. pMON999e35S-YFP was generously provided by G. van der Krogt.

Confocal microscopy and protoplast transfection

Cowpea (*Vigna unguiculata* L.) protoplasts were prepared and transfected with 10 μg of plasmid DNA using the polyethylene glycol method as described (van Bokhoven *et al.*, 1993). Samples were mounted 17 h after transfection in eight-chambered cover slides (Nalge Nunc International, Rochester, U.S.A.). Fluorescence microscopy was performed using a Zeiss LSM 510 confocal laser scanning microscope (CLSM; Carl-Zeiss, GmbH Germany) implemented on an inverted microscope (Axiovert 100). Excitation was provided by the 458- and 514-nm

Ar laser lines controlled by an acousto-optical tuneable filter (AOTF). Three dichroic beam splitters were used to separate excitation from emission and to divide the fluorescence emission into the CFP, YFP and chlorophyll channels. The HFT 458/514 dual dichroic beam splitter was used as a primary dichroic mirror reflecting excitation and transmitting fluorescence emission, an NFT 635 dichroic mirror was used as a secondary splitter and an NFT 515 was used as tertiary dichroic splitter. Fluorescence reflected by both the NFT 635 and NFT 515 splitters was filtered through a BP 470–500-nm filter yielding the CFP signal. Fluorescence reflected by the NFT 635 but transmitted by the NFT 515 splitter was filtered through a BP 530–600-nm filter yielding the YFP channel. Fluorescence transmitted by both the NFT 515 and 635 splitters was additionally filtered by an LP 650 filter to yield the chlorophyll image. Cross-talk-free CFP and YFP images were acquired by operating the microscope in the multitracking mode, in which the 514-nm excitation was coupled to activation of the YFP-detection channel, and the 458-nm excitation was coupled to activation of the CFP- and chlorophyll-detection channels. A Zeiss water immersion C-Apochromat 40× objective lens (NA 1.2) corrected for cover glass thickness (set at 0.16 μm for Nunc eight-chambered coverslides) was used for scanning. The detection pinholes were set at 2 Airy disk units. Images were captured and analysed with the Zeiss LSM510 software (v. 3.0 SP3).

FRET–FRAP

For FRET–FRAP, images were acquired on the Zeiss LSM510 microscope described above. After bleaching of a region of interest with maximum power using the 514-nm laser line, a time sequence of CFP and YFP images was acquired using the filter settings and multitracking mode as described above. Image analysis of plasma membrane fluorescence was performed with the public domain program Object-Image, an extended version of NIH-Image (see Vischer at http://simon.bio.uva.nl). The program supports non-destructive marking, vector overlay and 'detector regions', a technique in which suitably shaped search windows can be created and evaluated using local coordinate systems. For analysis, the images were arranged as a time series in the form of an image stack. In each stack slice, a ring-shaped region of interest was created whose inner and outer border extended to a distance of 1.5 μm on either side of the cell membrane. The ring was then radial-symmetrically subdivided into 18 ring segments. The mean intensities of the ring segments were measured and plotted vs. their angular positions. The plots were repeated for all images in the time series.

FLIM

For frequency-domain wide-field FLIM measurements, the FLIM/SPIM set-up implemented on an inverted fluorescence microscope (Axiovert 200M, Zeiss, Germany) as described by van Munster & Gadella (2004) was used. For selective imaging of CFP, a helium–cadmium laser (442 nm, 125 mW, Melles-Griot, U.S.A.) for excitation, a 455DCLP dichroic mirror and a D480/40 bandpass emission filter (Chroma, U.S.A.) were used. The frequency of the modulation was 74.818 MHz. Reference phase and modulation were obtained using a reference filter cube reflecting 0.1‰ of the excitation laser light directly on to the detector (van Munster & Gadella, 2004). FLIM stacks of eight phase images were acquired with an exposure time of 0.5–1 s each using a Zeiss plan Neofluar 40× 1.3 NA, oil-immersion objective. Protoplasts were mounted in eight-chambered cover slides (Nalge Nunc International). Photobleaching of CFP was not found to be a problem.

FSPIM

For FSPIM measurements the same FLIM/SPIM set-up was used as described by van Munster & Gadella (2004). A 100-W mercury-arc lamp and a D436/20 nm excitation filter provided excitation. For spectral analysis a 20/80% reflection/transmission dichroic mirror and an HQ460LP emission filter (both from Chroma) were used. On the side port of the microscope an imaging spectrograph (Imspector V7, Specim, Finland) coupled to a CCD camera (ORCA ER, Hamamatsu, Japan) was mounted for spectral detection. For all experiments the Zeiss plan Neofluar 40× 1.3 NA, oil-immersion objective was used. For this objective, the slit dimensions corresponded to 201 μm × 2 μm in the object plane. The wavelength axis of the image spectra was calibrated using the mercury lines of the excitation source. The response function of the spectrograph and camera was calibrated using a calibration source (QTH 20W, Oriel, U.S.A). Software for control, acquisition, processing and analysis of the data was written in C++, using Matlab 6.1 (The Mathworks, U.S.A.) and the image-processing library DIPlib (Pattern Recognition Group, TU Delft, the Netherlands, http://www.ph.tn.tudelft.nl/DIPlib/).

Results

Membrane targeting of CFP-Zm7hvr and myrLeCPK1-YFP

Ivanchenko *et al.* (2000) and Rutschmann *et al.* (2002) showed that GFP fused to the HVR of the maize ROP7 or to the N-myristoylation motif of LeCPK1 is sufficient to target the GFP to the plasma membrane. To study both constructs in the same cell we fused the HVR of the maize ROP7 to the C-terminus of CFP (CFP-Zm7hvr) and fused the myristoylation sequence of LeCPK1 to the N-terminus of YFP (myrLeCPK1-YFP). These constructs were transiently co-expressed in cowpea mesophyll protoplasts and showed a similar labelling of the plasma membrane in comparison with the observations by Ivanchenko *et al.* (2000) and Rutschman *et al.* (2002) (Fig. 1a,b). As expected, in protoplasts co-expressing CFP-Zm7hvr and unfused YFP, there was a clear difference in localization between CFP-Zm7hvr

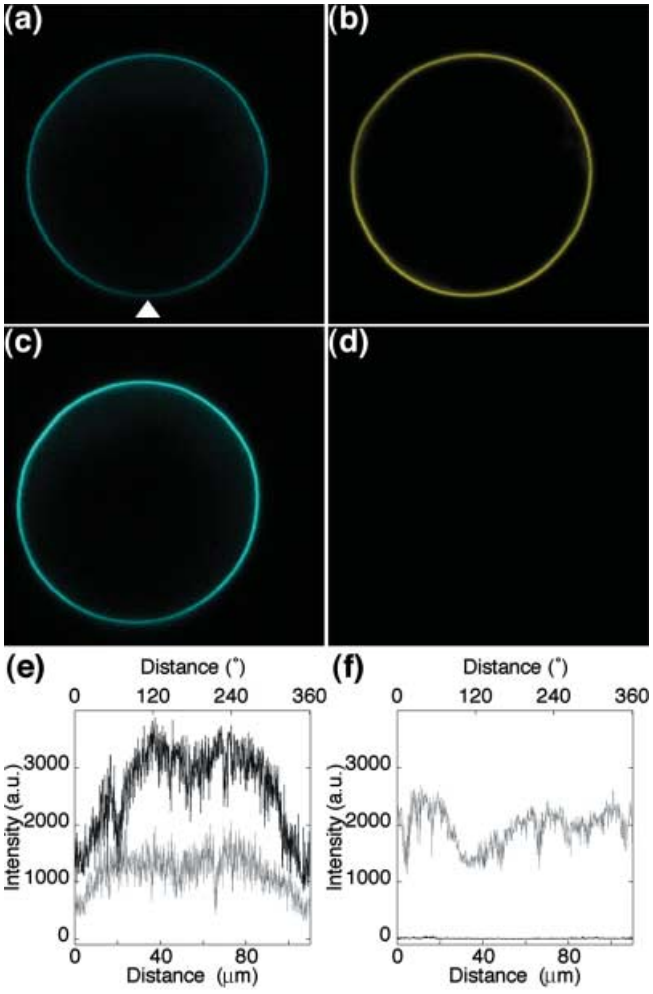

Fig. 1. Confocal fluorescence image of cowpea protoplasts co-expressing CFP-Zm7hvr and myrLeCPK1-YFP before (a,b) and after acceptor-photobleaching (c,d). The quantified fluorescence intensity of the plasma membrane before and after acceptor-photobleaching is depicted for CFP-Zm7hvr (e) and for myrLeCPK1-YFP (f). In (e) and (f) the grey curve represents the plasma membrane fluorescence intensity before acceptor-photobleaching and black curve represents the plasma membrane fluorescence intensity after acceptor-photobleaching. The arrowhead indicates the 0° point, from where the plots in (e) and (f) begin (clockwise rotation). Scale bar is identical to the scale bar in Fig. 2.

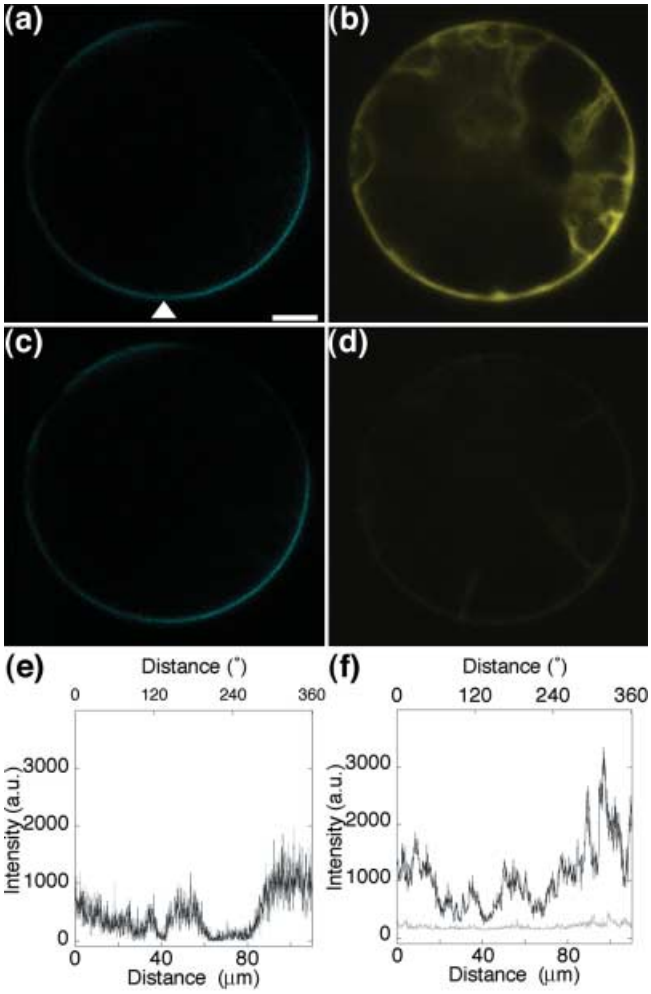

Fig. 2. Confocal fluorescence image of a cowpea protoplast co-expressing CFP-Zm7hvr and YFP before (a,b) and after acceptor-photobleaching (c,d). The quantified fluorescence intensity of the plasma membrane before and after acceptor-photobleaching is depicted for CFP-Zm7hvr (e) and for YFP (f). The grey curve represents the plasma membrane fluorescence intensity before acceptor-photobleaching and black curve represents the plasma membrane fluorescence intensity after acceptor-photobleaching. The arrowhead indicates the 0° point, from where the plots in (e) and (f) begin (clockwise rotation). Scale bar = 10 μm.

and YFP (Fig. 2a,b). The fluorescence at the plasma membrane was quantified as a function of distance by image processing methods. The fact that some areas at the plasma membrane (0°–60° and 300°–360°) appear to be less labelled by CFP and more uniformly by YFP is caused by severe inner-filtering of the CFP fluorescence by chloroplasts near the membrane area.

Acceptor bleaching FRET microscopy

In view of the perfect co-localization of the CFP-Zm7hvr and myrLeCPK1-YFP, their possible interaction in plasma membrane lipid microdomains was investigated using acceptor bleaching FRET microscopy. As a control myrLeCPK1-YFP was replaced by unfused YFP. MyrLeCPK1-YFP (Fig. 1b) or unfused YFP (Fig. 2b) were photobleached with 514-nm laser light and the post-bleaching CFP image was taken directly after bleaching the YFP. Figures 1(c) and 2(c) show the post-bleaching CFP and YFP images corresponding to Figs 1(a,b) and 2(a,b). From the lack of YFP fluorescence in the post-bleach image it was inferred that the YFP bleaching was close to 100%. Interestingly, as clearly seen from a comparison of Fig. 1(a) and Fig. 1(c), there was an increase of donor, CFP-Zm7hvr, fluorescence after bleaching of myrLeCPK1-YFP. The quantified fluorescence intensity at the plasma membrane (Fig. 1e) clearly shows that the CFP fluorescence intensity was

increased over the entire plasma membrane region and was elevated on average 2.35-fold. Using Eq. (1), this indicated that there was an average FRET efficiency of 58% at the plasma membrane. By contrast, for the control protoplast co-expressing the CFP-Zm7hvr and unfused YFP no concomitant increase of CFP fluorescence was observed despite quantitative bleaching of the YFP (see Fig. 2e), indicating the lack of FRET.

FSPIM/FLIM-analysis

Because the bleaching experiments indicated that there was FRET in protoplasts co-expressing CFP-Zm7hvr and myrLeCPK1-YFP, we employed FSPIM and FLIM microscopy to validate the acceptor bleaching experiments and to cross-compare the different FRET methods. First, fluorescence emission spectra were taken to determine if there was sensitized emission in protoplasts co-expressing CFP-Zm7hvr and myrLeCPK1-YFP and to compare these spectra with the spectra from protoplasts co-expressing CFP-Zm7hvr and unfused YFP. Figure 3 shows the average spectra of the plasma membrane area of eight protoplasts co-expressing CFP-Zm7hvr and myrLeCPK1-YFP or those co-expressing CFP-Zm7hvr and unfused YFP. For comparison, spectra of protoplasts expressing only CFP-Zm7hvr are also shown. All spectra were normalized to the fluorescence observed at 475 nm (i.e. the first emission band of CFP). Figure 3 shows that upon 435-nm excitation there was a strong YFP fluorescence emission in protoplasts co-expressing

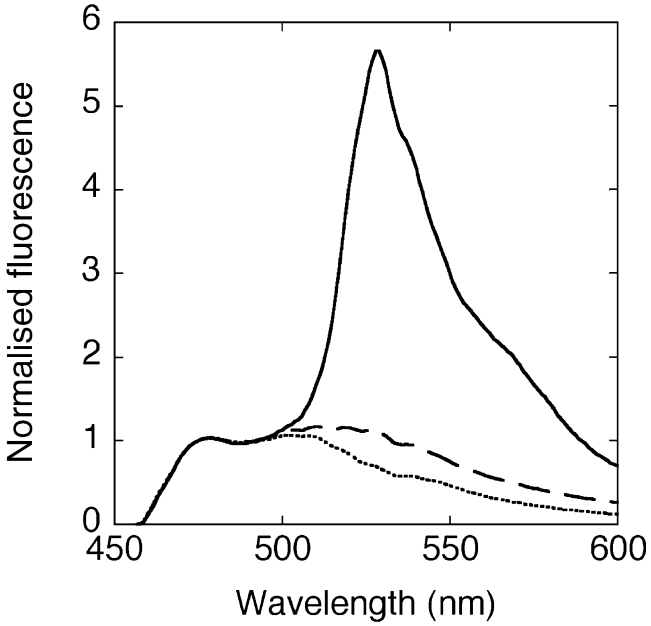

Fig. 3. FSPIM analysis of protoplasts co-expressing CFP-Zm7hvr and myrLeCPK1-YFP (continuous line), CFP-Zm7hvr and YFP (dashed line) or only CFP-Zm7hvr (dotted line). Image spectra were taken using 435-nm excitation light. The background-corrected but otherwise uncorrected fluorescence spectra are normalized to the intensity observed at 475 nm. Each curve represents the mean spectrum for eight individual protoplasts.

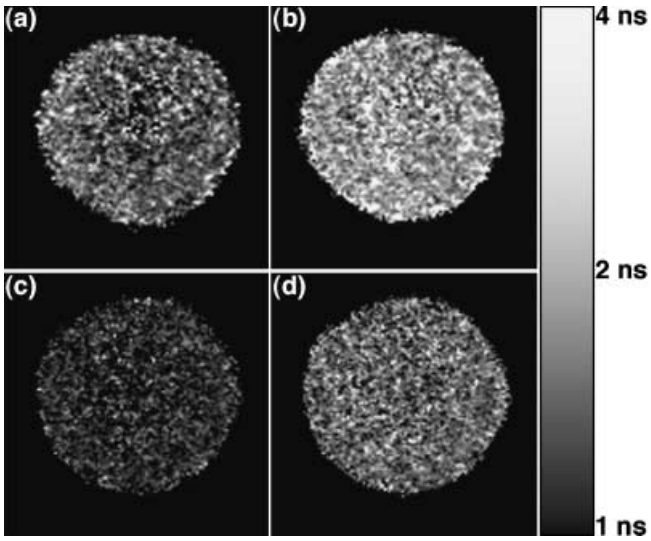

Fig. 4. FLIM analysis of cowpea protoplasts co-expressing CFP-Zmhvr7 and YFP (a,b), or CFP-Zm7hvr and myrLeCPK1-YFP (c,d). Images (a) and (c) are micrographs of τ_ϕ, whereas (b) and (d) are micrographs of τ_M. The mean values of τ_ϕ and τ_M are 2.13 ns, 2.81 ns, 1.41 ns and 2.13 ns for images (a)–(d), respectively. The lifetime values are indicated in a greyscale ranging from black (1 ns) to white (4 ns) as indicated next to the figure.

CFP-Zm7hvr and myrLeCPK1-YFP (from 500 to 600 nm), but there was almost no YFP fluorescence observed in protoplasts co-expressing CFP-Zm7hvr and unfused YFP. The large extent of sensitized YFP emission in the presence of myrLeCPK1-YFP clearly confirms the FRET data obtained with the acceptor bleaching experiments. The small amount of YFP fluorescence shown in the protoplasts co-expressing CFP-Zm7hvr and unfused YFP is due to slight residual direct excitation of YFP at 435 nm.

Subsequently, we employed FLIM microscopy on several protoplasts co-expressing the FRET couple and the control couple. Figure 4 shows the average phase (τ_ϕ) and modulation (τ_M) fluorescence lifetimes of a protoplast co-expressing CFP-Zm7hvr and YFP (Fig. 4a,b) and a protoplast co-expressing CFP-Zm7hvr and myrLeCPK1-YFP (Fig. 4c,d). The protoplasts co-expressing CFP-Zm7hvr and myrLeCPK1-YFP showed a decreased donor (CFP) lifetime in comparison with protoplasts co-expressing CFP-Zm7hvr and unfused YFP (compare Fig. 4a,b with Fig. 4c,d). On average the τ_ϕ and the τ_M of the protoplasts co-expressing CFP-Zm7hvr and myrLeCPK1-YFP were 1.56 ± 0.11 ns ($n = 8$) and 2.31 ± 0.20 ns ($n = 8$), respectively, whereas for control protoplasts co-expressing CFP-Zm7hvr and unfused YFP they were 2.14 ± 0.10 ns ($n = 8$) and 2.81 ± 0.03 ns ($n = 8$), respectively. From these values, using Eq. (1), average FRET efficiencies of 28% from τ_ϕ and 18% from τ_M were determined. These percentages for the FRET efficiency are much lower than the FRET efficiency observed with the bleaching experiments, which can be explained by the fact that FLIM is biased towards the longer lifetime components in the case of heterogeneous FRET (see Discussion).

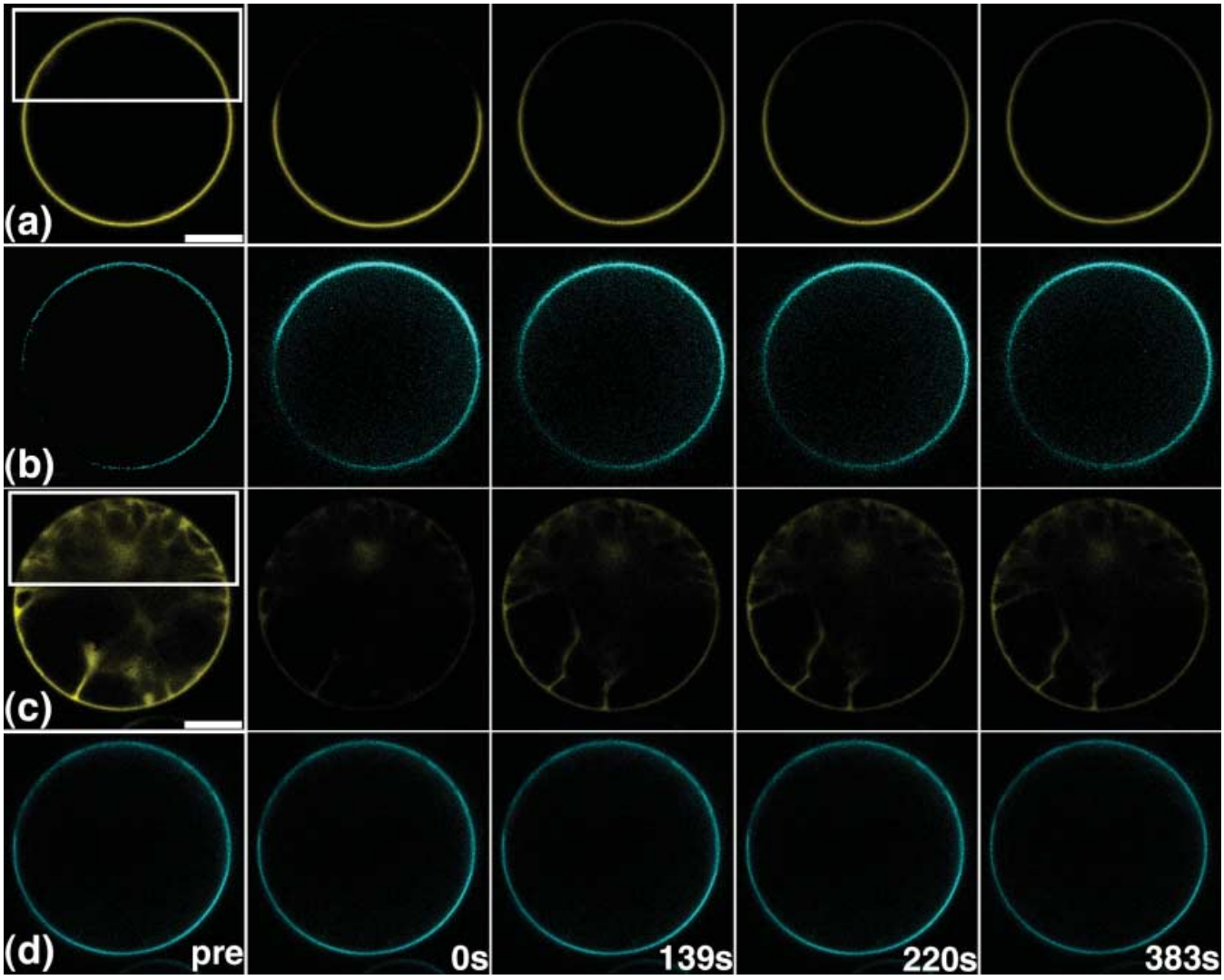

Fig. 5. FRET–FRAP analysis of cowpea protoplasts co-expressing myrLeCPK1-YFP and CFP-Zmhvr7 (a,b, respectively), or unfused YFP and CFP-Zm7hvr (c,d, respectively). The acceptor-photobleached area is indicated by the rectangle in the left subimage (a) and (c). Scale bar = 10 μm.

FRET–FRAP analysis

In order to investigate the stability of the complex between CFP-Zmhvr7 and myrLeCPK1-YFP, we performed a FRET–FRAP measurement. With FRET–FRAP, first the acceptor is photobleached in part of the cell, resulting in dequenching of the donor. Subsequently, the kinetics of requenching of the donor by association with the unbleached acceptor is measured. In this way, the stability of the complex can be assessed because requenching of the donor means that its bleached associated partner (acceptor) molecule is exchanged for a non-bleached partner. In the case of a very stable complex, the kinetics of requenching will be slow whereas for a less stable complex the kinetics of CFP requenching will be fast. Figure 5(a,b) show a FRET–FRAP time series of a protoplast co-expressing CFP-Zm7hvr and myrLeCPK1-YFP followed in time after acceptor-bleaching. It is clear from Fig. 5(b) that there was a strong increase in donor fluorescence after bleaching of the acceptor but that as a function of time the CFP-Zm7hvr fluorescence becomes requenched again at the plasma membrane owing to redistribution of non-photobleached acceptors. By contrast, upon acceptor-bleaching in a protoplast co-expressing CFP-Zm7hvr and unfused YFP (Fig. 5c,d) not only is the boxed area acceptor-bleached but rather the whole protoplast is bleached, owing to the fact that the unfused YFP is cytosolic and hence diffuses much faster. Clearly, in this control experiment the CFP-Zm7hvr fluorescence was unaltered during bleaching and recovery of the YFP fluorescence. Figure 6 shows the quantified recovery of the plasma membrane CFP and YFP fluorescence intensity of a partially acceptor-photobleached protoplast. Figure 6(a,b) correspond to images Fig. 5(a,b) and Fig. 5(c,d), respectively. In both cases the plasma membrane

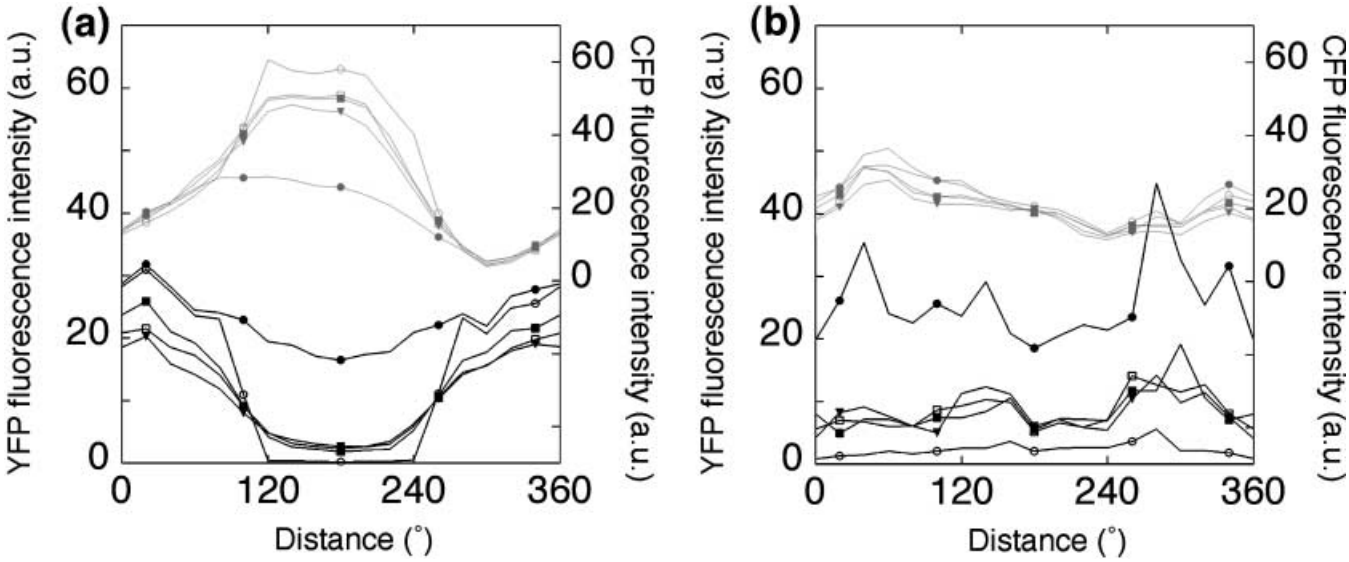

Fig. 6. FRET–FRAP image analysis of Fig. 5. Panel (a) corresponds to Fig. 5(a,b) whereas panel (b) corresponds to Fig. 5(c,d). The CFP and YFP fluorescence intensity at the plasma membrane is depicted in grey and black, respectively. The measurement starts at the same point as indicated by the arrowhead in Figs 1(a) and 2(a) but continues anticlockwise. Line markers: closed circles, prebleaching; open circles, 0 s; closed squares, 139 s; open squares, 220 s; closed triangles, 381 s after acceptor-photobleaching.

region between approximately 120° and 240° is acceptor-photobleached. It is clear from Fig. 6(a) that exactly in the bleached area, there was a strong increase of CFP fluorescence (compare the curves with open and closed circle symbols). For the control protoplast this increase was negligible (Fig. 6b). Figure 6(a) also shows that recovery of myrLeCPK1-YFP fluorescence into the bleached area (120°–240°) requenches the CFP-Zm7 fluorescence. However, the decrease in YFP in the areas from 0° to 120° and from 240° to 360° due to diffusion is not accompanied by a partial unquenching of CFP-Zm7hvr, indicating the presence of higher-order complexes (see Discussion).

Discussion

Multimode FRET microscopy was applied to study plasma membrane lipid microdomains in plant protoplasts. We used acceptor-photobleaching FRET microscopy, FSPIM and FLIM in cowpea protoplasts co-expressing lipidated CFP- and YFP-fusions. We showed that all techniques indicated that there was FRET between CFP-Zm7hvr and myrLeCPK1-YFP and hence that all techniques can be used to study protein–protein interactions in living plant cells.

However, the FLIM- and acceptor-bleaching FRET methods provided different apparent FRET efficiencies. These discrepancies are partly due to a different weighing of the data (Gadella *et al.*, 1994) and the multi-exponential nature of the decay of CFP (Pepperkok *et al.*, 1999; van Kuppeveld *et al.*, 2002). In the case of a multi-exponential decaying donor in a non-FRET situation, its fluorescence intensity is proportional to its lifetime contributions according to:

$$I_D = \sum_i a_i \tau_{i,D} \tag{3}$$

in which a_i is the relative amplitude of the ith exponentially decaying component with lifetime $\tau_{i,D}$. In the presence of an acceptor and proportional quenching of all lifetime components $\tau_{i,DA}$ by a factor $1 - E$ the intensity of the donor is given by:

$$I_{DA} = \sum_i a_i \tau_{i,DA} = \sum_i a_i \tau_{i,D}(1 - E) = (1 - E) I_D. \tag{4}$$

For frequency-domain lifetime imaging the weighing factors are more complicated (Weber, 1981; Jameson *et al.*, 1984; Gadella *et al.*, 1994):

$$\tau_\phi = \frac{\sum_i \dfrac{\alpha_i \tau_{i,D}}{1 + (\omega \tau_{i,D})^2}}{\sum_i \dfrac{\alpha_i}{1 + (\omega \tau_{i,D})^2}}$$

and

$$\tau_M = \frac{1}{\omega} \left(\frac{1}{\left(\sum_i \dfrac{\alpha_i \omega \tau_{i,D}}{1 + (\omega \tau_{i,D})^2} \right)^2 + \left(\dfrac{\alpha_i}{1 + (\omega \tau_{i,D})^2} \right)^2} - 1 \right)^{1/2} \tag{5}$$

where α_i is the fractional contribution ($\Sigma_i \alpha_i \equiv 1$) to the steady-state fluorescence made by the ith emitting species with lifetime $\tau_{i,D}$ and ω is the angular frequency of modulation ($\omega = 2\pi f$). Hence $\alpha_i \equiv a_i \tau_{i,D} / \Sigma_i a_i \tau_{i,D}$ and thus:

$$\tau_\phi = \frac{\sum_i \frac{a_i \tau_{i,D}^2}{1+(\omega\tau_{i,D})^2}}{\sum_i \frac{a_i \tau_{i,D}}{1+(\omega\tau_{i,D})^2}} \quad \text{and}$$

$$\tau_M = \frac{1}{\omega}\left(\frac{\left(\sum_i a_i \tau_{i,D}\right)^2}{\left(\sum_i \frac{\alpha_i \omega \tau_{i,D}^2}{1+(\omega\tau_{i,D})^2}\right)^2 + \left(\frac{a_i \tau_{i,D}}{1+(\omega\tau_{i,D})^2}\right)^2} - 1\right)^{1/2}. \qquad (6)$$

This results in a weighing in which for multiple lifetime components $\tau_{\phi,D} < \tau_{M,D}$ and typically that longer lifetime components contribute more extensively to $\tau_{M,D}$ than to $\tau_{\phi,D}$. Regardless, in the case of homogeneous FRET (equivalent quenching of all lifetime components) of a multi-exponentially decaying donor, the discrepancy between the 58% FRET-efficiency determined from the acceptor bleaching (using Eqs 1, 3 and 4) and the 28% and 18% apparent efficiencies determined from $\tau_{\phi,D}$ and $\tau_{M,D}$, respectively, is too large to be explained solely by a multi-exponential decaying donor. Hence, we suggest that the discrepancy in the estimated FRET efficiencies arises from a mixture of a population of donors being almost completely quenched and a population of non-quenched donors. The non-quenched population of donors contributes most prominently to the residual donor fluorescence in the presence of the acceptor and hence contributes extensively to $\tau_{M,DA}$ and to a lesser extent to $\tau_{\phi,DA}$, whereas the almost completely quenched donor population contributes most to the acceptor-bleach FRET estimation. This results in an underestimation of the true FRET efficiency from the $\tau_{\phi,DA}$ and $\tau_{M,DA}$ lifetimes as compared to the acceptor-bleach FRET-estimation. This apparent discrepancy can be understood if we assume the following lifetime components, relative contributions and population sizes. If we assume that CFP in the absence of the acceptor has two lifetime components $\tau_{1,D} = 1.3$ ns and $\tau_{2,D} = 4.0$ ns, with relative contributions of 67% and 33%, respectively ($a_1 = 0.67$ and $a_2 = 0.33$) according to Eq. (6) we obtain $\tau_{\phi,D} = 2.15$ ns and $\tau_{M,D} = 2.83$ ns (and an average lifetime $\bar{\tau}_D \equiv \Sigma_i a_i \tau_{i,D} / \Sigma_i a_i = 2.19$ ns), chosen as to compare favourably with the measured values. If we assume a population of 33% of the CFP being unquenched in the presence of the acceptor coexisting with a population of 67% of the CFP being quenched for 87% by the acceptor, we have a four-component exponential decay with $\tau_{1,DA} = 1.3$ ns, $\tau_{2,DA} = 4.0$ ns, $\tau_{3,DA} = 0.17$ ns and $\tau_{4,DA} = 0.52$ ns with relative contributions of $a_1 = 0.22$, $a_2 = 0.11$, $a_3 = 0.45$ and $a_4 = 0.22$, respectively. In this case, Eq. (6) (substituting τ_{DA} for τ_D) yields $\tau_{\phi,DA} = 1.46$ ns, $\tau_{M,DA} = 2.42$ ns and $\bar{\tau}_{DA} = 0.92$ ns, again in agreement with the experimental values. Hence in this case $E \equiv 1 - \bar{\tau}_{DA}/\bar{\tau}_D$ would be 58% (in agreement with the acceptor bleach data), $E_\phi \equiv 1 - \tau_{\phi,DA}/\tau_{\phi,D} = 32\%$ and $E_M \equiv 1 - \tau_{M,DA}/\tau_{M,D} = 15\%$. Although the numbers in this example have been chosen relatively arbitrarily, this example clearly illustrates that in the case of a mixture of nearly totally quenched donor and unquenched donor, different energy transfer efficiencies are estimated from the different techniques displaying the trend: $E > E_\phi > E_M$ corresponding to our experimental data. The idea that part of the donor is almost completely quenched and a part is unquenched is compatible with the existence of lipid microdomains in the plasma membrane. In such microdomains lipidated CFP and YFP are tightly packed, resulting in strongly quenched CFP owing to FRET to multiple acceptors, whereas in other microdomains they both could be relatively less concentrated, yielding unquenched CFP fluorescence. The numerical illustration above using a four-component exponential decay is probably very oversimplified. In reality, a distribution involving many more lifetime components for populations of CFPs FRET-ing to no, one, two, three and multiple acceptors is more likely and, hence, the numerical example should be seen as a dual-component dual-population simplification of reality. For this reason, attempts to perform fits to multi-exponentials using multiple-frequency data (Squire *et al.*, 2000) or global analysis of single-frequency data assuming discrete lifetime components (Verveer *et al.*, 2000a) (both beyond the scope of this paper) were not attempted on our FLIM data.

Interestingly, from a more detailed analysis (using the new image analysis tools) of the plasma membrane fluorescence intensity of a partially acceptor-bleached protoplast as depicted in Fig. 6(a), the above notions are supported. Clearly, CFP becomes requenched upon diffusion of non-bleached lipidated YFP into the acceptor-bleached area. Strikingly, in the areas where YFP was not bleached (0°–120° and 240°–360°) one can see no increase in CFP fluorescence, despite the decrease in YFP fluorescence resulting from its redistribution. This means that a portion of the acceptor (YFP) can leave the FRET complex without changing the intensity of the donor. In our opinion this result again illustrates that there are multiple acceptors in the FRET complex, and that disappearance of a few of them hardly affects the CFP quenching. Together with the very slow recovery rates (half-lives of several minutes) the data suggest the existence of relatively stable higher-order complexes of lipidated GFPs in the plasma membrane microdomains. Clearly, the FRET–FRAP findings corroborate the FLIM data as discussed above. This underlines the advantage of multimodal FRET microscopy because in combination far more information can be extracted than from one technique alone.

There have been extensive reports regarding the existence of plasma membrane microdomains in mammalian cells (Zacharias *et al.*, 2002) and also reports for plants (Peskan *et al.*, 2000). Yet the existence of lipid microdomains or rafts in plasma membranes of plants is open to debate. Currently, a more extensive study is being carried out using more differentially lipidated GFPs in different combinations to obtain more conclusive evidence for the occurrence, behaviour and biological significance of lipid microdomains in plants.

Acknowledgements

We would like to acknowledge Dr J. E. Fowler (Oregon State University, Corvallis, U.S.A.) for the pMG-GFP-Zm7hvr plasmid and Dr J. Goedhart for stimulating discussions and critical reading of the manuscript. J.E.M.V. was supported by the Council for Earth and Life Sciences (ALW), project number 810-66.012.

References

Balaban, R.S., Kurtz, I., Cascio, H.E. & Smith, P.D. (1986) Microscopic spectral imaging using a video camera. *J. Microsc.* **141**, 31–39.

Bastiaens, P.I., Majoul, I.V., Verveer, P.J., Soling, H.D. & Jovin, T.M. (1996) Imaging the intracellular trafficking and state of the AB5 quaternary structure of cholera toxin. *EMBO J.* **15**, 4246–4253.

Bastiaens, P.I. & Squire, A. (1999) Fluorescence lifetime imaging microscopy: spatial resolution of biochemical processes in the cell. *Trends Cell Biol.* **9**, 48–52.

van Bokhoven, H., Verver, J., Wellink, J. & van Kammen, A. (1993) Protoplasts transiently expressing the 200K coding sequence of cowpea mosaic virus B-RNA support replication of M-RNA. *J. Gen. Virol.* **74**, 2233–2241.

Clayton, A.H., Hanley, Q.S., Arndt-Jovin, D.J., Subramaniam, V. & Jovin, T.M. (2002) Dynamic fluorescence anisotropy imaging microscopy in the frequency domain (rFLIM). *Biophys. J.* **83**, 1631–1649.

Clegg, R.M. (1996) Fluorescence resonance energy transfer. *Fluorescence Imaging Spectroscopy and Microscopy* (ed. by X.-F. Wang), pp. 179–252. John Wiley and Sons, Chichester.

Creemers, T.M., Lock, A.J., Subramaniam, V., Jovin, T.M. & Volker, S. (2000) Photophysics and optical switching in green fluorescent protein mutants. *Proc. Natl Acad. Sci. USA*, **97**, 2974–2978.

Dhonukshe, P. & Gadella, T.W. Jr (2003) Alteration of microtubule dynamic instability during preprophase band formation revealed by yellow fluorescent protein-CLIP170 microtubule plus-end labeling. *Plant Cell*, **15**, 597–611.

Gadella, T.W.J. Jr (1997) Fluorescence lifetime imaging microscopy (FLIM): instrumentation and applications. *Fluorescent and Luminescent Probes for Biological Activity* (ed. by W. T. Mason), pp. 467–479. Academic Press, London.

Gadella, T.W. Jr, Clegg, R.M. & Jovin, T.M. (1994) Fluorescence lifetime imaging microscopy: pixel-by-pixel analysis of phase-modulation data. *Bioimaging*, **2**, 139–159.

Gadella, T.W.J. Jr & Jovin, T.M. (1995) Oligomerization of epidermal growth factor receptors on A431 cells studied by time-resolved fluorescence imaging microscopy. A stereochemical model for tyrosine kinase receptor activation. *J. Cell Biol.* **129**, 1543–1558.

Gadella, T.W.J. Jr, van der Krogt, G.N. & Bisseling, T. (1999) GFP-based FRET microscopy in living plant cells. *Trends Plant Sci.* **4**, 287–291.

Gadella, T.W.J. Jr, Vereb, G. Jr, Hadri, A.E., Rohrig, H., Schmidt, J., John, M., Schell, J. & Bisseling, T. (1997) Microspectroscopic imaging of nodulation factor-binding sites on living *Vicia sativa* roots using a novel bioactive fluorescent nodulation factor. *Biophys. J.* **72**, 1986–1996.

Gautier, I., Tramier, M., Durieux, C., Coppey, J., Pansu, R.B., Nicolas, J.C., Kemnitz, K. & Coppey-Moisan, M. (2001) Homo-FRET microscopy in living cells to measure monomer–dimer transition of GFP-tagged proteins. *Biophys. J.* **80**, 3000–3008.

Glomset, J.A. & Farnsworth, C.C. (1994) Role of protein modification reactions in programming interactions between ras-related GTPases and cell membranes. *Annu. Rev. Cell Biol.* **10**, 181–205.

Goedhart, J. & Gadella, T.W.J. Jr (2000) Advanced fluorescence microspectroscopic methods for the study of single living root hairs. *Root Hairs: Cellular and Molecular Biology* (ed. by R. W. Ridge & A. M. C. Emons), pp. 65–94. Springer, Tokyo.

Gordon, G.W., Berry, G., Liang, X.H., Levine, B. & Herman, B. (1998) Quantitative fluorescence resonance energy transfer measurements using fluorescence microscopy. *Biophys. J.* **74**, 2702–2713.

Hanley, Q.S., Subramaniam, V., Arndt-Jovin, D.J. & Jovin, T.M. (2001) Fluorescence lifetime imaging: multi-point calibration, minimum resolvable differences, and artifact suppression. *Cytometry*, **43**, 248–260.

Harpur, A.G., Wouters, F.S. & Bastiaens, P.I. (2001) Imaging FRET between spectrally similar GFP molecules in single cells. *Nat. Biotechnol.* **19**, 167–169.

Honda, A., Adams, S.R., Sawyer, C.L., Lev-Ram, V., Tsien, R.Y. & Dostmann, W.R. (2001) Spatiotemporal dynamics of guanosine 3′,5′-cyclic monophosphate revealed by a genetically encoded, fluorescent indicator. *Proc. Natl Acad. Sci. USA*, **98**, 2437–2442.

Immink, R.G., Gadella, T.W.J. Jr, Ferrario, S., Busscher, M. & Angenent, G.C. (2002) Analysis of MADS box protein–protein interactions in living plant cells. *Proc. Natl Acad. Sci. USA*, **99**, 2416–2421.

Ivanchenko, M., Vejlupkova, Z., Quatrano, R.S. & Fowler, J.E. (2000) Maize ROP7 GTPase contains a unique, CaaX box-independent plasma membrane targeting signal. *Plant J.* **24**, 79–90.

Jameson, D.M., Gratton, E. & Hall, R.D. (1984) The measurement and analysis of heterogeneous emission by multifrequency phase and modulation fluorometry. *Appl. Spectrosc. Rev.* **20**, 55–106.

Janetopoulos, C., Jin, T. & Devreotes, P. (2001) Receptor-mediated activation of heterotrimeric G-proteins in living cells. *Science*, **291**, 2408–2411.

Karpova, T.S., Baumann, C.T., He, L., Wu, X., Grammer, A., Lipsky, P., Hager, G.L. & McNally, J.G. (2003) Fluorescence resonance energy transfer from cyan to yellow fluorescent protein detected by acceptor photobleaching using confocal microscopy and a single laser. *J. Microsc.* **209**, 56–70.

Kenworthy, A.K. (2001) Imaging protein–protein interactions using fluorescence resonance energy transfer microscopy. *Methods*, **24**, 289–296.

van Kuppeveld, F.J., Melchers, W.J., Willems, P.H. & Gadella, T.W. Jr (2002) Homomultimerization of the coxsackievirus 2B protein in living cells visualized by fluorescence resonance energy transfer microscopy. *J. Virol.* **76**, 9446–9456.

Magee, T. & Marshall, C. (1999) New insights into the interaction of Ras with the plasma membrane. *Cell*, **98**, 9–12.

Michaelson, D., Silletti, J., Murphy, G., D'Eustachio, P., Rush, M. & Philips, M.R. (2001) Differential localization of Rho GTPases in live cells: regulation by hypervariable regions and RhoGDI binding. *J. Cell Biol.* **152**, 111–126.

Miyawaki, A., Llopis, J., Heim, R., McCaffery, J.M., Adams, J.A., Ikura, M. & Tsien, R.Y. (1997) Fluorescent indicators for Ca^{2+} based on green fluorescent proteins and calmodulin. *Nature*, **388**, 882–887.

van Munster, E.B. & Gadella, T.W.J. Jr (2004) ϕFLIM: a new method to avoid aliasing in frequency-domain fluorescence lifetime imaging microscopy. *J. Microsc.*, **213**, 29–38.

Pepperkok, R., Squire, A., Geley, S. & Bastiaens, P.I. (1999) Simultaneous detection of multiple green fluorescent proteins in live cells by fluorescence lifetime imaging microscopy. *Curr. Biol.* **9**, 269–272.

Peskan, T., Westermann, M. & Oelmuller, R. (2000) Identification of low-density Triton X-100-insoluble plasma membrane microdomains in higher plants. *Eur. J. Biochem.* **267**, 6989–6995.

Rutschmann, F., Stalder, U., Piotrowski, M., Oecking, C. & Schaller, A. (2002) LeCPK1, a calcium-dependent protein kinase from tomato. Plasma membrane targeting and biochemical characterization. *Plant Physiol.* **129**, 156–168.

Sambrook, J. & Russel, D.W. (2001) *Molecular Cloning: A Laboratory Manual.* Cold Spring Harbor Laboratory Press, Cold Spring Harbor, NY.

Selvin, P.R. (2000) The renaissance of fluorescence resonance energy transfer. *Nat. Struct. Biol.* **7**, 730–734.

Sorkin, A., McClure, M., Huang, F. & Carter, R. (2000) Interaction of EGF receptor and grb2 in living cells visualized by fluorescence resonance energy transfer (FRET) microscopy. *Curr. Biol.* **10**, 1395–1398.

Squire, A., Verveer, P.J. & Bastiaens, P.I. (2000) Multiple frequency fluorescence lifetime imaging microscopy. *J. Microsc.* **197**, 136–149.

Stryer, L. (1978) Fluorescence energy transfer as a spectroscopic ruler. *Annu. Rev. Biochem.* **47**, 819–846.

Tsien, R.Y. (1998) The green fluorescent protein. *Annu. Rev. Biochem.* **67**, 509–544.

Verveer, P.J., Squire, A. & Bastiaens, P.I. (2000a) Global analysis of fluorescence lifetime imaging microscopy data. *Biophys. J.* **78**, 2127–2137.

Verveer, P.J., Wouters, F.S., Reynolds, A.R. & Bastiaens, P.I. (2000b) Quantitative imaging of lateral ErbB1 receptor signal propagation in the plasma membrane. *Science*, **290**, 1567–1570.

van der Wal, J., Habets, R., Varnai, P., Balla, T. & Jalink, K. (2001) Monitoring agonist-induced phospholipase C activation in live cells by fluorescence resonance energy transfer. *J. Biol. Chem.* **276**, 15337–15344.

Weber, G. (1981) Resolution of the fluorescence lifetimes in a heterogeneous system by phase and modulation measurements. *J. Phys. Chem.* **85**, 945–953.

Wouters, F.S. & Bastiaens, P.I. (1999) Fluorescence lifetime imaging of receptor tyrosine kinase activity in cells. *Curr. Biol.* **9**, 1127–1130.

Zaccolo, M., De Giorgi, F., Cho, C.Y., Feng, L., Knapp, T., Negulescu, P.A., Taylor, S.S., Tsien, R.Y. & Pozzan, T. (2000) A genetically encoded, fluorescent indicator for cyclic AMP in living cells. *Nat. Cell Biol.* **2**, 25–29.

Zacharias, D.A., Violin, J.D., Newton, A.C. & Tsien, R.Y. (2002) Partitioning of lipid-modified monomeric GFPs into membrane microdomains of live cells. *Science*, **296**, 913–916.